
TESSER: Transfer-Enhancing Adversarial Attacks from Vision Transformers via Spectral and Semantic Regularization

Amira Guesmi
 NYU Abu Dhabi
 UAE
 ag9321@nyu.edu

Bassem Ouni
 Technology Innovation Institute
 UAE
 Bassem.Ouni@tii.ae

Muhammad Shafique
 NYU Abu Dhabi
 UAE
 ms12713@nyu.edu

Abstract

Adversarial transferability remains a critical challenge in evaluating the robustness of deep neural networks. In security-critical applications, transferability enables black-box attacks without access to model internals, making it a key concern for real-world adversarial threat assessment. While Vision Transformers (ViTs) have demonstrated strong adversarial performance, existing attacks often fail to transfer effectively across architectures, especially from ViTs to Convolutional Neural Networks (CNNs) or hybrid models. In this paper, we introduce **TESSER** — a novel adversarial attack framework that enhances transferability via two key strategies: (1) *Feature-Sensitive Gradient Scaling (FSGS)*, which modulates gradients based on token-wise importance derived from intermediate feature activations, and (2) *Spectral Smoothness Regularization (SSR)*, which suppresses high-frequency noise in perturbations using a differentiable Gaussian prior. These components work in tandem to generate perturbations that are both semantically meaningful and spectrally smooth. Extensive experiments on ImageNet across 12 diverse architectures demonstrate that TESSER achieves +10.9% higher attack success rate (ASR) on CNNs and +7.2% on ViTs compared to the state-of-the-art Adaptive Token Tuning (ATT) method. Moreover, TESSER significantly improves robustness against defended models, achieving 53.55% ASR on adversarially trained CNNs. Qualitative analysis shows strong alignment between TESSER’s perturbations and salient visual regions identified via Grad-CAM, while frequency-domain analysis reveals a 12% reduction in high-frequency energy, confirming the effectiveness of spectral regularization.

1 Introduction

Deep learning models, particularly Convolutional Neural Networks (CNNs) and Vision Transformers (ViTs), have achieved state-of-the-art performance across a broad spectrum of computer vision tasks [2, 49, 22]. Despite this progress, these models remain highly vulnerable to adversarial examples — carefully crafted perturbations that are imperceptible to humans but cause misclassification [10, 12–14]. In safety-critical applications such as autonomous driving and medical imaging, this fragility raises significant security concerns.

Although white-box attacks, where attackers have full access to model parameters, have been extensively studied, black-box settings are more realistic in practice. These are based on the principle of *transferability*, where adversarial examples generated on a surrogate model are expected to fool unseen target models. However, transferability across architectures, especially from ViTs to CNNs or hybrid models, remains limited due to two key challenges: (1) the lack of **semantic selectivity**, where all tokens are perturbed uniformly without considering their relevance to the model’s prediction, and

(2) the presence of **high-frequency noise** in perturbations, which tends to encode brittle, model-specific artifacts that do not generalize well.

Several recent works, such as ATT [24] and TGR [48], have explored ViT-specific mechanisms for improving transferability by truncating or regularizing gradient flows. However, these approaches either use fixed gradient masks or overlook token-level semantics, leading to suboptimal alignment with transferable visual features. In this paper, we introduce **TESSER** (*Transfer-Enhancing Semantic and Spectral Regularization*) a novel adversarial attack framework specifically designed to improve black-box transferability from ViT-based models to a diverse set of architectures. TESSER integrates two complementary strategies:

Feature-Sensitive Gradient Scaling (FSGS): a token-level gradient modulation method that scales gradients based on token importance derived from intermediate embeddings. Inspired by recent findings correlating token activation magnitudes with semantic relevance [19, 41, 25], FSGS steers the attack toward semantically meaningful regions and away from background or non-informative tokens, enhancing cross-model generalization.

Spectral Smoothness Regularization (SSR): a lightweight regularization mechanism that applies a differentiable Gaussian blur during each optimization step. SSR suppresses high-frequency noise, promoting low-frequency perturbations that are more resilient across architectures, particularly beneficial when transferring to CNNs and adversarially trained models.

Together, these modules enable TESSER to produce perturbations that are semantically aligned and spectrally smooth, two characteristics that we empirically demonstrate to be critical for enhancing transferability in adversarial attacks.

Our main contributions are summarized as follows:

- We propose **TESSER**, a novel adversarial attack framework that combines semantic- and spectral-aware regularization to improve transferability from ViTs.
- We introduce Feature-Sensitive Gradient Scaling (FSGS), which reweights gradients for Attention, QKV, and MLP modules based on token-level importance, encouraging semantically aligned perturbations.
- We incorporate Spectral Smoothness Regularization (SSR) to reduce high-frequency noise and enhance cross-architecture generalization.
- We conduct extensive experiments on ImageNet across 12 diverse models (including ViTs, CNNs, and adversarially defended CNNs), demonstrating that TESSER achieves up to **+10.9%** higher ASR over state-of-the-art baselines and consistently outperforms existing attacks in both black-box and robust scenarios.
- We conduct comprehensive ablation studies, Grad-CAM-based semantic alignment evaluations (Section 4.4), and frequency-domain analyses (Section 4.5) to demonstrate both the effectiveness and interpretability of our approach.

2 Related Work

Adversarial Attacks on CNNs and ViTs. Adversarial attacks are small, human-imperceptible perturbations intentionally added to input data to mislead deep learning models [10]. For Convolutional Neural Networks (CNNs), numerous gradient-based attacks have been proposed to improve transferability, including momentum-based methods [4], variance tuning [18], and gradient skipping techniques [40]. These methods aim to stabilize perturbation updates and avoid local optima in the input space. However, attack techniques designed for CNNs do not transfer well to Vision Transformers (ViTs), which have fundamentally different architectures and information flow patterns. Recent works have proposed ViT-specific attacks that exploit token structure and attention mechanisms [26, 38]. For example, Token Gradient Regularization (TGR) [48] modifies intermediate-layer gradients to reduce token-wise variance, improving transferability within ViT families.

Regularizing gradients is an effective way to suppress model-specific patterns and improve cross-model generalization. In CNNs, methods like SGM [40] and BPA [42] aim to manipulate the gradient flow through skip connections or rectify distortions introduced by nonlinearities. Others have employed gradient variance reduction [18] and ensemble-based tuning [44]. Attacks based on feature

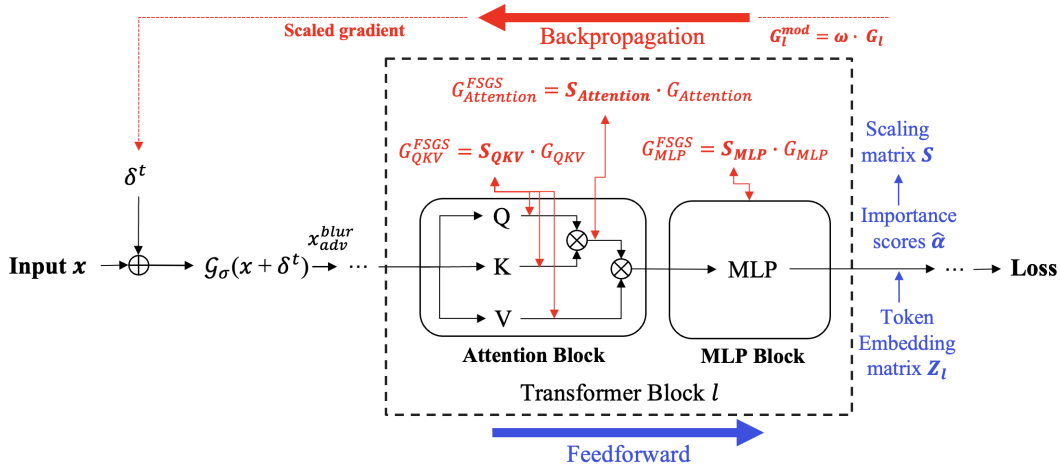


Figure 1: **Overview of the TESSER attack framework.** At each iteration, an adversarial perturbation δ^t is applied to the input image and smoothed via differentiable Gaussian blur $\mathcal{G}_\sigma(\cdot)$ to enforce spectral smoothness (SSR). The perturbed input is passed through the transformer, where token embeddings Z_l from each layer are used to compute token-wise importance scores $\hat{\alpha}$, which in turn define gradient scaling masks S . During backpropagation, gradients for the Attention, QKV, and MLP modules are reweighted according to their respective scaling masks ($S_{\text{Attention}}, S_{\text{QKV}}, S_{\text{MLP}}$) using Feature-Sensitive Gradient Scaling (FSGS). This encourages perturbations to align with semantically meaningful and transferable features while suppressing noise and irrelevant gradients.

information [37, 9] focus on disrupting salient internal representations. However, improperly guided feature-based attacks risk discarding useful information and reducing transferability. To mitigate this, neuron attribution methods [48] and attention map diversification [28] have been explored, particularly in ViTs. ATT [24] introduces hybrid token gradient truncation by weakening gradients in attention and QKV blocks across layers of a ViT model. It leverages empirical observations of gradient variance to suppress high-magnitude gradients associated with overfitting, thereby improving transferability. However, ATT applies static truncation and does not explicitly consider token-level semantic relevance, which may limit its effectiveness when generalizing across diverse architectures. In contrast, our method introduces *Feature-Sensitive Gradient Scaling (FSGS)*, which adaptively reweights gradients at a token level based on feature norms. This allows us to preserve semantically important gradients while suppressing noisy or architecture-specific ones, achieving improved transferability across ViTs, hybrids, and CNNs.

Input Diversity and Spectral Regularization. Input diversity has been widely adopted to improve adversarial transferability. DI-FGSM [43] applies random resizing and padding, while PatchOut [38] discards patch-wise perturbations to prevent overfitting. Recent self-paced extensions further refine patch discarding based on semantic guidance [24]. While these approaches diversify the spatial patterns of inputs, few works address the frequency structure of perturbations. Our method incorporates *Spectral Smoothness Regularization (SSR)* by applying differentiable Gaussian blur during optimization. SSR suppresses high-frequency noise and promotes smooth perturbation patterns that generalize better across model architectures, particularly important for CNNs and early ViT layers that rely on localized features. **Importantly, input diversity is orthogonal to our method**, and can potentially be combined with TESSER for further gains. We provide additional results and analysis combining input diversity with our framework in the Appendix C.

3 Methodology

3.1 Preliminaries

Let $\mathbf{x} \in \mathbb{R}^{C \times H \times W}$ denote an input image with ground-truth label $y \in \{1, 2, \dots, K\}$, and let $f(\cdot)$ be a deep neural network classifier. The goal of an untargeted adversarial attack is to generate a perturbation δ such that the perturbed input $\mathbf{x}^{\text{adv}} = \mathbf{x} + \delta$ is misclassified by the model, i.e.,

$f(\mathbf{x}^{\text{adv}}) \neq y$, while ensuring that $\|\delta\|_\infty \leq \epsilon$. Unlike CNNs that process local image regions hierarchically, Vision Transformers [7] operate on a sequence of non-overlapping image patches. Given an input image \mathbf{x} , it is partitioned into $N = \frac{HW}{P^2}$ patches of size $P \times P$, each linearly projected to a D -dimensional embedding, resulting in tokens $\{\mathbf{z}_1, \dots, \mathbf{z}_N\} \subset \mathbb{R}^D$. A learnable classification token \mathbf{z}_{cls} is prepended, yielding a token sequence $\mathbf{Z}^{(0)} \in \mathbb{R}^{(N+1) \times D}$, which is enriched with positional encodings. ViTs consist of a stack of L transformer blocks. Each block contains a Multi-Head Self-Attention (MHSA) module and a Multi-Layer Perceptron (MLP) module, connected via residual connections and layer normalization (LN).

The effectiveness of an attack depends on how well the crafted perturbation generalizes across architectures. In this work, we design an attack method that targets the attention, QKV, and MLP modules explicitly, and introduces gradient- and frequency-based regularization strategies to improve transferability across ViTs, hybrids, and CNNs.

3.2 Feature-Sensitive Gradient Scaling (FSGS)

To improve transferability, we propose *Feature-Sensitive Gradient Scaling (FSGS)*, a fine-grained gradient modulation strategy that steers adversarial updates toward semantically relevant tokens while suppressing gradients associated with model-specific or noisy patterns. Unlike prior methods such as ATT [24] and TGR [48], which rely on fixed truncation or uniform regularization, FSGS leverages intermediate transformer features to dynamically adjust gradient flow on a per-token basis.

Limitations of Prior Gradient Modulation Approaches. ATT weakens gradients across transformer modules based on empirical variance, but applies static masks that may disregard salient tokens. TGR promotes token-wise gradient uniformity without regard for token semantics, leading to potentially ineffective or redundant updates. In contrast, FSGS introduces adaptive scaling conditioned on the importance of each token, measured directly from the model’s internal activations. This content-aware reweighting enhances the alignment of perturbations with generalizable visual features and improves cross-architecture transfer.

Token-Level Importance Estimation. Given a token embedding matrix $\mathbf{Z} \in \mathbb{R}^{T \times D}$, we estimate the importance of token i using the activation norm $\alpha_i = \|\mathbf{z}_i\|_2$, which serves as a proxy for semantic saliency. This assumption is supported by prior work in both NLP and vision [19, 41, 25], which shows that activation magnitudes often correlate with token informativeness or attention saliency. For instance, Kobayashi et al. [19] and Wang et al. [25] argue that vector norms contribute substantially to a token’s influence, while Wu et al. [41] highlight the role of transformed token magnitudes in ViT explanations. These scores are min-max normalized:

$$\hat{\alpha}_i = \frac{\alpha_i - \min_j \alpha_j}{\max_j \alpha_j - \min_j \alpha_j + \varepsilon}$$

where ε ensures numerical stability.

Gradient Reweighting. Each token’s gradient is modulated by a scaling factor:

$$s_i = \gamma_{\text{base}} + \lambda(1 - \hat{\alpha}_i), \quad \mathbf{g}_i^{\text{FSGS}} = s_i \cdot \mathbf{g}_i$$

Here, $\gamma_{\text{base}} \in (0, 1]$ ensures minimum gradient flow, while λ controls the suppression strength for less important tokens. This reweighting selectively amplifies gradients linked to semantically meaningful content. FSGS is applied independently to the QKV projections, attention weights, and MLP layers, using module-specific hyperparameters $\lambda_{\text{qkv}}, \lambda_{\text{attn}}, \lambda_{\text{mlp}}$, allowing tailored control over each component. FSGS is implemented via backward hooks, imposes negligible overhead, and integrates seamlessly with iterative attack frameworks. By aligning perturbations with high-importance regions, it enhances the semantic coherence and transferability of adversarial examples across both homogeneous and heterogeneous architectures.

Semantic Gradient Preservation. In Vision Transformers, each token contributes to the final prediction through self-attention, MLP transformations, and CLS-token pooling. The gradient of the loss with respect to a token’s embedding indicates how much that token influences the model’s output. FSGS leverages the activation norm of intermediate token embeddings as a proxy for semantic importance: Higher activation norms typically correspond to visually meaningful content such as object boundaries, textures, or salient regions [21, 41]. By preserving gradients associated with these high-importance tokens and suppressing those from less informative or background areas, FSGS

steers adversarial perturbations toward features that are more likely to generalize across architectures. This selective modulation avoids wasting the attack budget on noisy or model-specific components, thereby improving transferability.

To validate this design intuition, we compute Grad-CAM [30] heatmaps using the incorrect (adversarial) predictions of the black-box model and analyze their spatial alignment with perturbations generated by FSGS. Interestingly, even though the model misclassifies the input, the resulting Grad-CAM activations still highlight semantically meaningful regions (e.g., object boundaries or foreground), suggesting that FSGS preserves gradients aligned with true semantic features. This supports our hypothesis that activation norm correlates with token importance and that FSGS steers perturbations toward generalizable, transferable regions. See Section 4.4 for qualitative visualizations and Appendix A for further analysis.

3.3 Spectral Smoothness Regularization (SSR)

In addition to feature-aware gradient modulation, we introduce *Spectral Smoothness Regularization (SSR)* to suppress high-frequency perturbation artifacts that often limit cross-architecture transferability. SSR operates by applying a differentiable Gaussian blur to the adversarial input at each iteration, effectively enforcing a low-pass filter on the evolving perturbation. Let δ denote the adversarial perturbation and $\mathcal{G}_\sigma(\cdot)$ the Gaussian blur operator with standard deviation σ . The input passed to the model becomes: $\mathbf{x}_{adv}^{blur} = \mathcal{G}_\sigma(\mathbf{x} + \delta)$. The intuition behind SSR is grounded in observations from both signal processing and adversarial transferability literature: perturbations dominated by high-frequency components tend to overfit to surrogate model-specific features and fail to generalize across architectures [35, 46]. By enforcing spectral smoothness, we bias the perturbation towards lower frequencies, which are more likely to align with perceptually salient and transferable features.

Unlike input diversity methods [43] that rely on stochastic resizing or padding to enhance transferability, SSR deterministically constrains the spectral characteristics of the perturbation itself. It is also fundamentally different from smoothing-based defenses, as the blur is applied *during optimization* rather than at test time, making it an attack-side regularizer. SSR is computationally efficient, introduces no additional parameters, and is compatible with any gradient-based attack pipeline. In our implementation, we integrate SSR into each PGD iteration following the perturbation update step. As shown in our experiments, SSR synergizes with FSGS to improve attack success rates, especially in black-box settings and when transferring across model families with divergent inductive biases.

3.4 Module-Wise Gradient Modulation

Vision Transformers differ from CNNs not only in architecture but also in how features and gradients evolve with depth. Prior studies [24, 47, 26] have shown that deeper transformer layers tend to encode more specialized, model-specific patterns (particularly in the attention maps) which can harm the transferability of adversarial perturbations. To address this, we introduce a *Module-wise gradient modulation* strategy that suppresses unstable gradients in deep attention layers and softly attenuates the gradient flow in all modules (Attention, QKV, MLP) based on their layer depth. Inspired by ATT [24], our approach consists of two key components:

Selective Attention Truncation. We truncate the gradients flowing through the *Attention module* for deep transformer blocks beyond a fixed threshold l_{cut} , by setting their attention gradients to zero: $\mathbf{g}_l^{attn} \leftarrow \mathbb{1}_{[l < l_{cut}]} \cdot \mathbf{g}_l^{attn}$. This effectively disables attention backpropagation in deeper layers, mitigating overfitting to model-specific global patterns.

Module-Wise Gradient Weakening. For all layers $l \in \{1, \dots, L\}$ and modules $m \in \{\text{attn}, \text{qkv}, \text{mlp}\}$, we scale the gradients using a module-specific weakening factor $\omega^{(m)} \in (0, 1]$: $\mathbf{g}_l^{(m)} \leftarrow \omega^{(m)} \cdot \mathbf{g}_l^{(m)}$. This softly adjusts the contribution of each module based on its depth and functional role, before applying further refinement via FSGS. The weakening factors $\omega_m^{(l)}$ and the truncation layer threshold l_{cut} are predefined based on empirical sensitivity, further hyperparameter sensitivity studies are provided in Appendix D.

All gradient weakening and truncation operations are applied via backward hooks before the application of FSGS. This ordering ensures that noisy gradients are first suppressed or removed, and only the semantically meaningful signals are preserved and amplified by FSGS. Importantly, our method remains fully differentiable and does not alter the model’s forward pass, preserving compatibility

with any transformer backbone. The overall optimization algorithm and different hyper-parameters for training adversarial example are provided in Appendix B.

4 Experiments

4.1 Experiment Setup

Dataset. Following prior works [38, 48, 24], we randomly selected 1,000 clean images from the ILSVRC2012 validation set [29], ensuring that all surrogate models correctly classify each image with high confidence. This selection facilitates a consistent and fair evaluation of transferability across models.

Models. We employ four representative Vision Transformer models as surrogate architectures: ViT-B/16 [6], PiT-B [17], CaiT-S24 [34], and Visformer-S [3]. To assess cross-architecture generalization, we group evaluation into two categories: ViT-to-ViT and ViT-to-CNN transfer. For ViT-to-ViT, we use four unseen target ViTs: DeiT-B [33], TNT-S [15], LeViT-256 [11], and ConViT-B [8]. For ViT-to-CNN, we evaluate against four deep CNN models: Inception-v3 (Inc-v3), Inception-v4 (Inc-v4), Inception-ResNet-v2 (IncRes-v2), and ResNet-v2-152 (Res-v2) [31, 32, 16]. Additionally, to evaluate robustness against adversarial defenses, we include three adversarially trained models: Inc-v3-ens3, Inc-v4-ens4, and IncRes-v2-adv [23, 45].

Baselines. We compare our method against a suite of strong baseline attacks. These include momentum- and variance-based methods such as MI-FGSM (MIM) [5], VMI-FGSM (VMI) [36], and Skip Gradient Method (SGM) [39]. We also include three state-of-the-art transformer-specific attacks: PNA [38], TGR [48], and ATT [24], which incorporate attention structure or token-level heuristics into their gradient manipulation strategies. Our proposed method builds on this foundation by integrating token-sensitive gradient reweighting and spectral regularization.

Evaluation Metrics. We evaluate attack performance using the standard *Attack Success Rate* (ASR), defined as the proportion of adversarial examples that successfully fool the target model. Higher ASR (\uparrow) indicates stronger transferability.

Parameter Settings. All experiments use a maximum perturbation bound of $\epsilon = 16/255$, consistent with prior work [48]. The number of PGD iterations is set to $T = 10$, with a step size of $\eta = \epsilon/T = 1.6/255$. Momentum is used for stabilization with decay factor $\mu = 1.0$. Model- and method-specific hyperparameters follow their original settings unless otherwise stated. Input images are resized to 224×224 , and the patch size for transformer models is fixed at 16×16 . For spectral smoothness regularization, we apply Gaussian blur with fixed kernel size (3×3) and $\sigma = 0.5$. We set $\gamma_{\text{base}} = 0.5$. The weakening factors ω , layer truncation threshold l_{cut} , and the adaptive scaling factor to λ are tuned per model to balance the influence of QKV, Attention, and MLP gradients within the backward pass. The specific values of these hyperparameters are provided in Appendix B.

4.2 Evaluating the Transferability

We evaluate the black-box transferability of adversarial examples generated by TESSER across ViTs, CNNs, and adversarially defended CNNs. Table 1 shows results when attacking ViTs using ViT-based surrogates. TESSER achieves an average ASR of **86.88%**, outperforming the strongest baseline (ATT) by **+7.2%**. On CNN targets, where ViT-based attacks typically degrade, TESSER maintains strong performance with **74.4%** ASR **+10.9%** higher than ATT. This indicates that our semantic and frequency-aware perturbations generalize beyond transformer-specific structures. TESSER’s improvements are particularly notable on hybrid architectures like LeViT and ConViT, where both spatial alignment and cross-attention modeling are critical.

When facing adversarially trained CNNs (Table 2), TESSER achieves **53.55%** ASR, surpassing all baselines by a large margin. This suggests that TESSER generates perturbations that are not only transferable but also robust against strong defenses, an essential property for real-world attack scenarios. We also observe that the relative gains of TESSER vary across target types. For ViTs, the gains are moderate, likely because transformer-specific methods already perform reasonably well in this setting. However, the improvement is more pronounced on CNNs and defended CNNs, where ATT and TGR degrade significantly. This asymmetry suggests that our method is particularly effective at bridging the architectural gap between transformer and non-transformer models. Furthermore,

TESSER’s performance is more stable across all target types, showing lower variance than competing methods, which reinforces the robustness of our approach. Additional results and extended analysis are provided in Appendix C.

Table 1: The attack success rate (%) of various transfer-based attacks against eight ViT models and the average attack success rate (%) of all black-box models. The best results are highlighted in **bold**.

Model	Attack	ViT-B/16	PiT-B	CaiT-S/24	Visformer-S	DeiT-B	TNT-S	LeViT-256	ConViT-B	Avg _{bb}
ViT-B/16	MIM	100.0*	34.5	64.1	36.5	64.3	50.2	33.8	66.0	49.9
	VMI	99.6*	48.8	74.4	49.5	73.0	64.8	50.3	75.9	62.4
	SGM	100.0*	36.9	77.1	40.1	77.9	61.6	40.2	78.4	58.9
	PNA	100.0*	45.2	78.6	47.7	78.6	62.8	47.1	79.5	62.8
	TGR	100.0*	49.5	85.0	53.8	85.6	73.1	56.5	85.4	69.8
	ATT	99.9*	57.5	90.3	63.9	90.8	82.0	66.8	90.8	77.4
	Ours	100*	61.7	94	68.3	92.5	85.6	72.2	91.4	83.2 ↑
PiT-B	MIM	24.7	100.0*	34.7	44.5	33.9	43.0	38.3	37.8	36.7
	VMI	38.9	99.7*	51.0	56.6	50.1	57.0	52.6	51.7	51.1
	SGM	41.8	100.0*	57.3	73.9	57.9	72.6	68.1	59.9	61.6
	PNA	47.9	100.0*	62.6	74.6	62.4	70.6	67.3	61.7	63.9
	TGR	60.3	100.0*	80.2	87.3	78.0	87.1	81.6	76.5	78.7
	ATT	69.6	100.0*	86.1	91.9	85.5	93.5	89.0	85.5	85.9
	Ours	74.9	100.0*	91.6	93.2	92.1	95	92.4	91.7	91.4 ↑
CaiT-S/24	MIM	70.9	54.8	99.8*	55.1	90.2	76.4	54.8	88.5	70.1
	VMI	76.3	63.6	98.8*	67.3	88.5	82.3	67.0	88.1	76.2
	SGM	86.0	55.8	100.0*	68.2	97.7	91.1	74.9	96.7	81.5
	PNA	82.4	60.7	99.7*	67.7	95.7	86.9	67.1	94.0	79.2
	TGR	88.2	66.1	100.0*	75.4	98.8	92.8	74.7	97.9	84.8
	ATT	93.6	76.4	100.0*	85.9	99.4	96.9	87.4	98.8	91.2
	Ours	95.2	81.4	100*	90.3	99.6	97.5	90.7	98.9	94.2 ↑
Visformer-S	MIM	28.1	50.4	41.0	99.9*	36.9	51.9	49.4	39.6	42.5
	VMI	39.2	60.0	56.6	100.0*	54.1	62.8	59.1	54.4	55.2
	SGM	18.8	41.8	34.9	100.0*	31.2	52.1	52.7	29.5	37.3
	PNA	35.4	61.5	54.7	100.0*	51.0	66.3	64.5	50.7	54.9
	TGR	41.2	70.3	62.0	100.0*	59.5	74.7	74.8	56.2	62.7
	ATT	44.7	70.9	68.7	100.0*	66.4	78.8	80.9	58.4	67.0
	Ours	57.6	79.4	78.4	100.0*	75.9	83.2	85.3	69.6	78.7 ↑

4.3 Ablation on Module-Wise Gradient Modulation.

To understand the individual and combined contributions of our gradient modulation strategy across different transformer modules, we conduct an ablation study by selectively applying Feature-Sensitive Gradient Scaling to the Attention, QKV, and MLP components. Table 3 presents the attack success rates (ASR) on ViT-based models, CNNs, and defended CNNs under different configurations. When FSGS is applied to a single module, the Attention pathway contributes the most to transferability, particularly for ViTs, achieving an ASR of 80.1%. MLP-only and QKV-only configurations also yield strong improvements over the baseline, with notable gains on CNNs and defended models. Combining any two modules improves performance further, especially when including MLP, which significantly boosts ASR against robust models. The best results are obtained when FSGS is jointly applied to all three modules, yielding an ASR of 86.88% on ViTs and 53.55% on defended CNNs. These results confirm that our gradient modulation strategy is most effective when applied in a comprehensive and module-aware manner.

4.4 Qualitative Comparison: Perturbation Semantics

To further investigate the semantic alignment of perturbations generated by our method, we visualize adversarial examples produced by ATT [24] and our proposed FSGS. Each example includes the clean image, the adversarial image, and the corresponding Grad-CAM heatmap computed from the adversarial input using the predicted (incorrect) label of the black-box model. This setup allows us to examine whether the adversarial signal still localizes on meaningful regions of the input, despite successfully inducing misclassification. As shown in Figure 2, perturbations generated by FSGS exhibit high spatial alignment with semantically salient areas (often focusing on regions corresponding to object parts or discriminative textures) even when the model’s prediction is incorrect. This behavior suggests that FSGS preserves gradients associated with tokens that encode true class-relevant features. The resulting perturbations remain semantically grounded, in contrast to ATT, which tends to spread noise across the image without semantic focus.

Table 2: The attack success rate (%) of various transfer-based attacks against four undefended CNN models and three defended CNN models and the average attack success rate (%) of all black-box models. The best results are highlighted in **bold**.

Model	Attack	Inc-v3	Inc-v4	IncRes-v2	Res-v2	Inc-v3ens3	Inc-v3ens4	IncRes-v2adv	Avg _{bb}
ViT-B/16	MIM	31.7	28.6	26.1	29.4	22.3	19.8	16.5	24.9
	VMI	43.1	41.6	37.9	42.6	31.4	30.6	25.0	36.0
	SGM	31.5	27.7	23.8	28.2	20.8	18.0	14.3	23.5
	PNA	42.7	37.5	35.3	39.5	29.0	27.3	22.6	33.4
	TGR	47.5	42.3	37.6	43.3	31.5	30.8	25.6	36.9
	ATT	53.3	49.0	45.4	51.5	38.1	36.7	33.1	43.9
	Ours	63.4	59.6	54.4	57.7	48.6	49	42.3	53.6 ↑
PiT-B	MIM	36.3	34.8	27.4	29.6	19.0	18.3	14.1	25.6
	VMI	47.3	45.4	40.7	43.4	35.9	34.4	29.7	39.5
	SGM	50.6	45.4	38.4	41.9	25.6	20.8	16.7	34.2
	PNA	59.3	56.3	49.8	53.0	33.3	32.0	25.5	44.2
	TGR	72.1	69.8	65.1	64.8	43.6	41.5	32.8	55.7
	ATT	80.4	75.3	72.7	72.9	52.5	50.6	41.0	63.6
	Ours	87.2	87.5	78.4	80	61	61.3	48.9	72 ↑
CaiT-S/24	MIM	48.4	42.9	39.5	43.8	30.8	27.6	23.3	36.6
	VMI	58.5	50.9	48.2	52.0	38.1	36.1	30.1	44.8
	SGM	53.5	45.9	40.2	45.9	30.8	28.5	21.0	38.0
	PNA	57.2	51.8	47.7	51.6	38.4	36.2	30.1	44.7
	TGR	60.3	52.9	49.3	53.4	39.6	37.0	31.8	46.3
	ATT	73.9	66.0	66.3	66.4	54.6	52.1	43.9	60.5
	Ours	79.2	71.9	72	72.4	57.9	57.5	49.2	65.7 ↑
Visformer-S	MIM	44.5	42.5	36.6	39.6	24.4	20.5	16.6	32.1
	VMI	54.6	53.2	48.5	52.2	33.0	32.0	22.2	42.2
	SGM	43.2	41.1	29.6	35.7	16.1	13.0	8.2	26.7
	PNA	55.9	54.6	46.0	51.7	29.3	26.2	21.1	40.7
	TGR	65.9	66.8	55.3	60.9	36.0	32.5	23.3	48.7
	ATT	80.9	81.2	70.5	75.7	50.1	41.3	32.0	61.7
	Ours	84.2	84.6	77.3	80.6	64.6	57.4	45	70.5 ↑

Notably, this qualitative evidence also validates the central assumption underlying FSGS: that token activation norms correlate with semantic importance. Even when guided by the wrong prediction, the Grad-CAM heatmaps highlight regions that overlap with the object of interest (e.g., the bird), confirming that high-activation tokens contribute to visually meaningful features. By preserving such gradients, FSGS steers perturbations toward content that generalizes across architectures, improving both interpretability and black-box transferability.

4.5 Spectral Smoothness Evaluation via Frequency-Domain Analysis

Table 3: The average attack success rate (%) against ViTs, CNNs, and defended CNNs by our method with different module settings.

Attn	QKV	MLP	ViTs	CNNs	Def-CNNs
-	-	-	49.9	29.1	19.3
✓	-	-	80.1	61.1	36.1
-	✓	-	72.72	54.1	29.5
-	-	✓	71.87	59	36
✓	✓	-	78.43	55.4	30.3
✓	-	✓	83.32	70.9	52
-	✓	✓	81.21	66.3	39.9
✓	✓	✓	86.88	74.4	53.55

spectral concentration of different attack variants. Our results demonstrate that SSR substantially reduces the high-frequency energy of perturbations. Across examples, ATT shows the highest high-frequency ratios (e.g., 53-56%), while FSGS reduces this moderately ($\sim 52-55\%$). When combined with SSR, the high-frequency ratio drops further (to $\sim 45-47\%$), indicating smoother and more transferable perturbations. This confirms that SSR encourages low-frequency perturbation structure, complementing the token-aware gradient modulation of FSGS.

To quantitatively assess the effect of Spectral Smoothness Regularization (SSR), we conduct a frequency-domain analysis of the generated perturbations. Specifically, we compute the 2D Fast Fourier Transform (FFT) of each perturbation and evaluate the *high-frequency energy ratio*, defined as the proportion of energy outside the central low-frequency band in the log-magnitude spectrum (as shown in Figure 2). Given a perturbation $\delta \in \mathbb{R}^{3 \times H \times W}$, we compute its FFT, shift the spectrum to center the low frequencies, and apply a radial mask to isolate high-frequency components. This experiment is repeated on a batch of adversarial samples to compare the

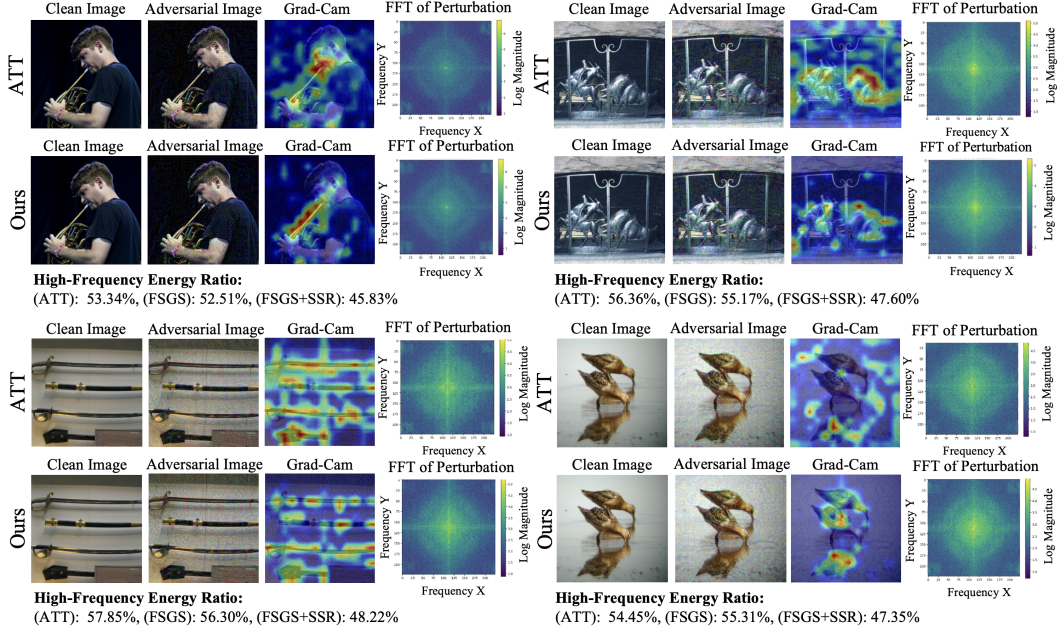


Figure 2: **Qualitative and frequency-domain comparison between ATT and our method (FSGS and FSGS + SSR).** Each row shows clean images, adversarial examples when using FSGS, Grad-CAM (guided by the adversarial label) overlays, and FFT log-magnitude spectra when using SSR. Our method produces perturbations that better align with semantically relevant regions and exhibit smoother frequency profiles. Further results and analysis are provided in Appendix D.

5 Conclusion

We proposed TESSER, a unified adversarial attack framework designed to improve transferability across diverse model architectures. By integrating Feature-Sensitive Gradient Scaling (FSGS) and Spectral Smoothness Regularization (SSR), TESSER guides adversarial gradients through semantically meaningful token activations and enforces smooth, low-frequency perturbation structures. Combined with layer and module-wise gradient modulation, our method effectively mitigates overfitting to model-specific representations and enhances generalization to unseen targets. Experimental results across a wide range of ViTs, hybrid models, and CNNs demonstrate that TESSER consistently outperforms state-of-the-art transfer attacks in both accuracy degradation and optimization efficiency.

6 Limitations and Broader Impact

Although our experimental results validate the effectiveness of the proposed Feature-Sensitive Gradient Scaling (FSGS) and Spectral Smoothness Regularization (SSR) in enhancing the transferability of ViT-based adversarial attacks, the underlying relationship between gradient sensitivity and transferability still lacks formal theoretical backing. Prior studies suggest that perturbations aligned with generalizable features tend to transfer better across models. Our work operationalizes this intuition by amplifying token importance and promoting gradient coherence to preserve semantically relevant signals, thereby improving black-box attack performance. In future work, we aim to explore this connection from a theoretical perspective to deepen our understanding of adversarial generalization.

This work aims to improve the evaluation of adversarial robustness by developing more transferable attacks across architectures. By revealing shared vulnerabilities in ViTs, CNNs, and hybrid models, our method can support the design of more generalizable defenses. However, improved transferability may also lower the barrier for black-box attacks. We emphasize that our approach is intended for academic use in robustness research, and encourage its application in developing safer, more resilient AI systems.

Acknowledgments and Disclosure of Funding

This research was partially funded by the Technology Innovation Institute (TII) under the “CASTLE: Cross-Layer Security for Machine Learning Systems IoT” project.

References

- [1] Samira Abnar and Willem Zuidema. Quantifying attention flow in transformers. *arXiv preprint arXiv:2005.00928*, 2020.
- [2] Nicolas Carion, Francisco Massa, Gabriel Synnaeve, Nicolas Usunier, Alexander Kirillov, and Sergey Zagoruyko. End-to-end object detection with transformers. In *European conference on computer vision*, pages 213–229. Springer, 2020.
- [3] Zhengsu Chen, Lingxi Xie, Jianwei Niu, Xuefeng Liu, Longhui Wei, and Qi Tian. Visformer: The vision-friendly transformer. In *Proceedings of the IEEE/CVF international conference on computer vision*, pages 589–598, 2021.
- [4] Yinpeng Dong, Fangzhou Liao, Tianyu Pang, Hang Su, Jun Zhu, Xiaolin Hu, and Jianguo Li. Boosting adversarial attacks with momentum. In *Proceedings of the IEEE conference on computer vision and pattern recognition*, pages 9185–9193, 2018.
- [5] Yinpeng Dong, Fangzhou Liao, Tianyu Pang, Hang Su, Jun Zhu, Xiaolin Hu, and Jianguo Li. Boosting adversarial attacks with momentum. In *Proceedings of the IEEE conference on computer vision and pattern recognition*, pages 9185–9193, 2018.
- [6] Alexey Dosovitskiy, Lucas Beyer, Alexander Kolesnikov, Dirk Weissenborn, Xiaohua Zhai, Thomas Unterthiner, Mostafa Dehghani, Matthias Minderer, Georg Heigold, Sylvain Gelly, et al. An image is worth 16x16 words: Transformers for image recognition at scale. *arXiv preprint arXiv:2010.11929*, 2020.
- [7] Alexey Dosovitskiy, Lucas Beyer, Alexander Kolesnikov, Dirk Weissenborn, Xiaohua Zhai, Thomas Unterthiner, Mostafa Dehghani, Matthias Minderer, Georg Heigold, Sylvain Gelly, Jakob Uszkoreit, and Neil Houlsby. An image is worth 16x16 words: Transformers for image recognition at scale, 2021. URL <https://arxiv.org/abs/2010.11929>.
- [8] Stéphane d’Ascoli, Hugo Touvron, Matthew L Leavitt, Ari S Morcos, Giulio Biroli, and Levent Sagun. Convit: Improving vision transformers with soft convolutional inductive biases. In *International conference on machine learning*, pages 2286–2296. PMLR, 2021.
- [9] Aditya Ganeshan, Vivek BS, and R Venkatesh Babu. Fda: Feature disruptive attack. In *Proceedings of the IEEE/CVF International Conference on Computer Vision*, pages 8069–8079, 2019.
- [10] Ian J. Goodfellow, Jonathon Shlens, and Christian Szegedy. Explaining and harnessing adversarial examples. *CoRR*, abs/1412.6572, 2014. URL <https://api.semanticscholar.org/CorpusID:6706414>.
- [11] Benjamin Graham, Alaaeldin El-Nouby, Hugo Touvron, Pierre Stock, Armand Joulin, Hervé Jégou, and Matthijs Douze. Levit: a vision transformer in convnet’s clothing for faster inference. In *Proceedings of the IEEE/CVF international conference on computer vision*, pages 12259–12269, 2021.
- [12] Amira Guesmi, Muhammad Abdullah Hanif, Bassem Ouni, and Muhammad Shafique. Physical adversarial attacks for camera-based smart systems: Current trends, categorization, applications, research challenges, and future outlook. *IEEE Access*, 11:109617–109668, 2023. doi: 10.1109/ACCESS.2023.3321118.
- [13] Amira Guesmi, Ruitian Ding, Muhammad Abdullah Hanif, Ihsen Alouani, and Muhammad Shafique. Dap: A dynamic adversarial patch for evading person detectors. In *Proceedings of the IEEE/CVF Conference on Computer Vision and Pattern Recognition (CVPR)*, pages 24595–24604, June 2024.
- [14] Amira Guesmi, Muhammad Abdullah Hanif, Ihsen Alouani, Bassem Ouni, and Muhammad Shafique. Ssap: A shape-sensitive adversarial patch for comprehensive disruption of monocular depth estimation in autonomous navigation applications. In *2024 IEEE/RSJ International Conference on Intelligent Robots and Systems (IROS)*, pages 2786–2793, 2024. doi: 10.1109/IROS58592.2024.10802252.
- [15] Kai Han, An Xiao, Enhua Wu, Jianyuan Guo, Chunjing Xu, and Yunhe Wang. Transformer in transformer. *Advances in neural information processing systems*, 34:15908–15919, 2021.
- [16] Kaiming He, Xiangyu Zhang, Shaoqing Ren, and Jian Sun. Deep residual learning for image recognition. In *Proceedings of the IEEE conference on computer vision and pattern recognition*, pages 770–778, 2016.

- [17] Byeongho Heo, Sangdoon Yun, Dongyoon Han, Sanghyuk Chun, Junsuk Choe, and Seong Joon Oh. Rethinking spatial dimensions of vision transformers. In *Proceedings of the IEEE/CVF international conference on computer vision*, pages 11936–11945, 2021.
- [18] Qian Huang, Isay Katsman, Horace He, Zeqi Gu, Serge Belongie, and Ser-Nam Lim. Enhancing adversarial example transferability with an intermediate level attack. In *Proceedings of the IEEE/CVF international conference on computer vision*, pages 4733–4742, 2019.
- [19] Goro Kobayashi, Tatsuki Kuribayashi, Sho Yokoi, and Kentaro Inui. Attention is not only a weight: Analyzing transformers with vector norms. *arXiv preprint arXiv:2004.10102*, 2020.
- [20] Xiao Lin and Devi Parikh. Leveraging visual question answering for image-caption ranking. In *Computer Vision—ECCV 2016: 14th European Conference, Amsterdam, The Netherlands, October 11–14, 2016, Proceedings, Part II 14*, pages 261–277. Springer, 2016.
- [21] Sifan Long, Zhen Zhao, Jimin Pi, Shengsheng Wang, and Jingdong Wang. Beyond attentive tokens: Incorporating token importance and diversity for efficient vision transformers. In *Proceedings of the IEEE/CVF Conference on Computer Vision and Pattern Recognition*, pages 10334–10343, 2023.
- [22] Fan Ma, Mike Zheng Shou, Linchao Zhu, Haoqi Fan, Yilei Xu, Yi Yang, and Zhicheng Yan. Unified transformer tracker for object tracking. In *Proceedings of the IEEE/CVF conference on computer vision and pattern recognition*, pages 8781–8790, 2022.
- [23] Aleksander Madry, Aleksandar Makelov, Ludwig Schmidt, Dimitris Tsipras, and Adrian Vladu. Towards deep learning models resistant to adversarial attacks. *arXiv preprint arXiv:1706.06083*, 2017.
- [24] Di Ming, Peng Ren, Yunlong Wang, and Xin Feng. Boosting the transferability of adversarial attack on vision transformer with adaptive token tuning. *Advances in Neural Information Processing Systems*, 37: 20887–20918, 2024.
- [25] Ali Modarressi, Mohsen Fayyaz, Yadollah Yaghoobzadeh, and Mohammad Taher Pilehvar. Globenc: Quantifying global token attribution by incorporating the whole encoder layer in transformers. *arXiv preprint arXiv:2205.03286*, 2022.
- [26] Muzammal Naseer, Kanchana Ranasinghe, Salman Khan, Fahad Shahbaz Khan, and Fatih Porikli. On improving adversarial transferability of vision transformers. *arXiv preprint arXiv:2106.04169*, 2021.
- [27] Maithra Raghu, Thomas Unterthiner, Simon Kornblith, Chiyuan Zhang, and Alexey Dosovitskiy. Do vision transformers see like convolutional neural networks? *Advances in neural information processing systems*, 34:12116–12128, 2021.
- [28] Yuchen Ren, Zhengyu Zhao, Chenhao Lin, Bo Yang, Lu Zhou, Zhe Liu, and Chao Shen. Improving adversarial transferability on vision transformers via forward propagation refinement, 2025. URL <https://arxiv.org/abs/2503.15404>.
- [29] Olga Russakovsky, Jia Deng, Hao Su, Jonathan Krause, Sanjeev Satheesh, Sean Ma, Zhiheng Huang, Andrej Karpathy, Aditya Khosla, Michael Bernstein, et al. Imagenet large scale visual recognition challenge. *International journal of computer vision*, 115:211–252, 2015.
- [30] Ramprasaath R Selvaraju, Michael Cogswell, Abhishek Das, Ramakrishna Vedantam, Devi Parikh, and Dhruv Batra. Grad-cam: Visual explanations from deep networks via gradient-based localization. In *Proceedings of the IEEE international conference on computer vision*, pages 618–626, 2017.
- [31] Christian Szegedy, Vincent Vanhoucke, Sergey Ioffe, Jon Shlens, and Zbigniew Wojna. Rethinking the inception architecture for computer vision. In *Proceedings of the IEEE conference on computer vision and pattern recognition*, pages 2818–2826, 2016.
- [32] Christian Szegedy, Sergey Ioffe, Vincent Vanhoucke, and Alexander Alemi. Inception-v4, inception-resnet and the impact of residual connections on learning. In *Proceedings of the AAAI conference on artificial intelligence*, volume 31, 2017.
- [33] Hugo Touvron, Matthieu Cord, Matthijs Douze, Francisco Massa, Alexandre Sablayrolles, and Hervé Jégou. Training data-efficient image transformers & distillation through attention. In *International conference on machine learning*, pages 10347–10357. PMLR, 2021.
- [34] Hugo Touvron, Matthieu Cord, Alexandre Sablayrolles, Gabriel Synnaeve, and Hervé Jégou. Going deeper with image transformers. In *Proceedings of the IEEE/CVF international conference on computer vision*, pages 32–42, 2021.

- [35] Dimitris Tsipras, Shibani Santurkar, Logan Engstrom, Alexander Turner, and Aleksander Madry. Robustness may be at odds with accuracy. *arXiv: Machine Learning*, 2018. URL <https://api.semanticscholar.org/CorpusID:52962648>.
- [36] Xiaosen Wang and Kun He. Enhancing the transferability of adversarial attacks through variance tuning. In *Proceedings of the IEEE/CVF conference on computer vision and pattern recognition*, pages 1924–1933, 2021.
- [37] Zhibo Wang, Hengchang Guo, Zhifei Zhang, Wenxin Liu, Zhan Qin, and Kui Ren. Feature importance-aware transferable adversarial attacks. In *Proceedings of the IEEE/CVF international conference on computer vision*, pages 7639–7648, 2021.
- [38] Zhipeng Wei, Jingjing Chen, Micah Goldblum, Zuxuan Wu, Tom Goldstein, and Yu-Gang Jiang. Towards transferable adversarial attacks on vision transformers. In *Proceedings of the AAAI Conference on Artificial Intelligence*, volume 36, pages 2668–2676, 2022.
- [39] Dongxian Wu, Yisen Wang, Shu-Tao Xia, James Bailey, and Xingjun Ma. Skip connections matter: On the transferability of adversarial examples generated with resnets. *arXiv preprint arXiv:2002.05990*, 2020.
- [40] Dongxian Wu, Yisen Wang, Shu-Tao Xia, James Bailey, and Xingjun Ma. Skip connections matter: On the transferability of adversarial examples generated with resnets. *arXiv preprint arXiv:2002.05990*, 2020.
- [41] Junyi Wu, Bin Duan, Weitai Kang, Hao Tang, and Yan Yan. Token transformation matters: Towards faithful post-hoc explanation for vision transformer. In *Proceedings of the IEEE/CVF Conference on Computer Vision and Pattern Recognition*, pages 10926–10935, 2024.
- [42] Wang Xiaosen, Kangheng Tong, and Kun He. Rethinking the backward propagation for adversarial transferability. *Advances in Neural Information Processing Systems*, 36:1905–1922, 2023.
- [43] Cihang Xie, Zhishuai Zhang, Yuyin Zhou, Song Bai, Jianyu Wang, Zhou Ren, and Alan L Yuille. Improving transferability of adversarial examples with input diversity. In *Proceedings of the IEEE/CVF conference on computer vision and pattern recognition*, pages 2730–2739, 2019.
- [44] Yifeng Xiong, Jiadong Lin, Min Zhang, John E Hopcroft, and Kun He. Stochastic variance reduced ensemble adversarial attack for boosting the adversarial transferability. In *Proceedings of the IEEE/CVF conference on computer vision and pattern recognition*, pages 14983–14992, 2022.
- [45] Zhuoer Xu, Guanghui Zhu, Changhua Meng, Zhenzhe Ying, Weiqiang Wang, Ming Gu, Yihua Huang, et al. A2: Efficient automated attacker for boosting adversarial training. *Advances in Neural Information Processing Systems*, 35:22844–22855, 2022.
- [46] Dong Yin, Raphael Gontijo Lopes, Jon Shlens, Ekin Dogus Cubuk, and Justin Gilmer. A fourier perspective on model robustness in computer vision. *Advances in Neural Information Processing Systems*, 32, 2019.
- [47] Jason Yosinski, Jeff Clune, Yoshua Bengio, and Hod Lipson. How transferable are features in deep neural networks? *Advances in neural information processing systems*, 27, 2014.
- [48] Jianping Zhang, Yizhan Huang, Weibin Wu, and Michael R Lyu. Transferable adversarial attacks on vision transformers with token gradient regularization. In *Proceedings of the IEEE/CVF conference on computer vision and pattern recognition*, pages 16415–16424, 2023.
- [49] Fangrui Zhu, Yi Zhu, Li Zhang, Chongruo Wu, Yanwei Fu, and Mu Li. A unified efficient pyramid transformer for semantic segmentation. In *Proceedings of the IEEE/CVF International Conference on Computer Vision*, pages 2667–2677, 2021.

Appendix

A Theoretical Justification of Feature-Sensitive Gradient Scaling (FSGS)

We provide a formal argument to support the hypothesis that modulating gradients based on token-level activation norms enhances adversarial transferability. Our analysis is grounded in the relationship between semantic informativeness and gradient alignment across models.

A.1 Preliminaries

Let $f : \mathbb{R}^d \rightarrow \mathbb{R}^K$ be a surrogate classifier and $f' : \mathbb{R}^d \rightarrow \mathbb{R}^K$ a target (black-box) classifier. An adversarial perturbation $\delta \in \mathbb{R}^d$ is added to input \mathbf{x} such that $\|\delta\|_\infty \leq \epsilon$ and $f(\mathbf{x} + \delta) \neq y$.

Assume \mathbf{x} is decomposed into T tokens with embeddings $\mathbf{z}_1, \dots, \mathbf{z}_T \in \mathbb{R}^D$. Denote the loss gradients w.r.t. each token as $\mathbf{g}_i = \nabla_{\mathbf{z}_i} \mathcal{L}(f(\mathbf{x}), y)$, and similarly for f' .

A.2 Semantic Tokens and Gradient Alignment

Let $S_{\text{sem}} \subseteq \{1, \dots, T\}$ be the set of semantically informative tokens (e.g., foreground object, discriminative parts). Let S_{bg} be its complement (background or irrelevant tokens).

We define the inter-model gradient alignment at token i as:

$$\text{Align}_i = \cos \theta_i = \frac{\langle \nabla_{\mathbf{z}_i} \mathcal{L}_f, \nabla_{\mathbf{z}_i} \mathcal{L}_{f'} \rangle}{\|\nabla_{\mathbf{z}_i} \mathcal{L}_f\| \cdot \|\nabla_{\mathbf{z}_i} \mathcal{L}_{f'}\|}$$

Assumption 1. *Gradients at semantically important tokens exhibit higher cross-model alignment:*

$$\mathbb{E}_{i \in S_{\text{sem}}} [\text{Align}_i] > \mathbb{E}_{i \in S_{\text{bg}}} [\text{Align}_i]$$

This is supported by empirical findings in model interpretability [1, 20, 27] and our own Grad-CAM visualizations (see Section 4.4).

A.3 Feature-Sensitive Gradient Scaling (FSGS)

FSGS assigns a scaling factor s_i to each token based on its activation norm $\alpha_i = \|\mathbf{z}_i\|_2$:

$$s_i = \gamma_{\text{base}} + \lambda(1 - \hat{\alpha}_i), \quad \hat{\alpha}_i = \frac{\alpha_i - \min_j \alpha_j}{\max_j \alpha_j - \min_j \alpha_j + \epsilon}$$

Tokens with high α_i (assumed to lie in S_{sem}) receive larger gradients, while low-importance tokens are suppressed.

Theorem 1 (FSGS Improves Expected Gradient Alignment). *Let $G = \sum_{i=1}^T \mathbf{g}_i$ be the unscaled gradient and $G_{\text{FSGS}} = \sum_{i=1}^T s_i \cdot \mathbf{g}_i$ the FSGS-scaled gradient. Under Assumption 1, the cosine alignment between G_{FSGS} and the target model’s gradient G' satisfies:*

$$\cos \theta(G_{\text{FSGS}}, G') > \cos \theta(G, G')$$

Sketch. We decompose the total gradient into two subsets:

$$G = \sum_{i \in S_{\text{sem}}} \mathbf{g}_i + \sum_{i \in S_{\text{bg}}} \mathbf{g}_i$$

FSGS scales $i \in S_{\text{sem}}$ by higher s_i than those in S_{bg} , thus:

$$G_{\text{FSGS}} = \sum_{i \in S_{\text{sem}}} s_i \mathbf{g}_i + \sum_{i \in S_{\text{bg}}} s_i \mathbf{g}_i$$

Since $\mathbb{E}_{i \in S_{\text{sem}}} [\text{Align}_i] > \mathbb{E}_{i \in S_{\text{bg}}} [\text{Align}_i]$, amplifying contributions from S_{sem} increases the expected alignment between G_{FSGS} and G' . Therefore:

$\cos \theta(G_{\text{FSGS}}, G') > \cos \theta(G, G')$ (by Jensen’s inequality over positively weighted aligned vectors) □

A.4 Implication

Theorem 1 provides theoretical support for the design of FSGS: boosting gradients from semantically salient tokens leads to improved alignment with gradients from unseen models, thereby enhancing adversarial transferability. This also explains the empirical advantage of FSGS in black-box settings, particularly when transferring from ViTs to CNNs or hybrid models.

B The Overall Framework of Optimization Algorithm

B.1 Algorithm

We now present the full optimization framework used to generate adversarial examples in our method. Our algorithm builds on the momentum-based PGD attack [4], and integrates three coordinated components: (1) *Module and Layer-Wise Gradient Modulation* to adjust the contribution of each transformer layer and suppress noisy deep-layer gradients, (2) *Feature-Sensitive Gradient Scaling (FSGS)* to selectively enhance semantically important token gradients, and (3) *Spectral Smoothness Regularization (SSR)* to constrain the perturbation’s frequency content.

Let $\mathbf{x} \in \mathbb{R}^{C \times H \times W}$ be a clean input, $y \in \{1, \dots, K\}$ its ground-truth label, and f the surrogate model. We seek a perturbation δ satisfying $\|\delta\|_\infty \leq \epsilon$, such that the adversarial input $\mathbf{x}^{\text{adv}} = \mathbf{x} + \delta$ misleads f and transfers effectively to other black-box models.

Optimization Procedure

The perturbation is optimized over T steps using projected gradient descent with momentum. At each step $t \in \{1, \dots, T\}$, the perturbed input is smoothed using a differentiable Gaussian blur operator:

$$\mathbf{x}^{(t)} = \mathcal{G}_\sigma(\mathbf{x} + \delta^{(t-1)})$$

where $\mathcal{G}_\sigma(\cdot)$ denotes Gaussian blurring with standard deviation σ , enforcing low-frequency spectral structure (SSR).

Next, the gradient of the loss is computed:

$$\mathbf{g}^{(t)} = \nabla_{\mathbf{x}} \mathcal{L}(f(\mathbf{x}^{(t)}), y)$$

This gradient is intercepted via backward hooks at key ViT modules (Attention, QKV, MLP). For each transformer block l , the following sequence is applied to each module:

1. **Module-wise Weakening:** The gradient $\mathbf{g}^{(l)}$ for each module is first scaled using a module-specific weakening factor $\omega^{(l)} \in (0, 1]$ (e.g., $\omega_{\text{attn}}^{(l)}, \omega_{\text{qkv}}^{(l)}, \omega_{\text{mlp}}^{(l)}$). This captures prior knowledge about the sensitivity of each module.
2. **Layer-wise Modulation:** The weakened attention gradient is then further modulated by a layer-specific coefficient $\tau_l \in [0, 1]$, which reduces the influence of deeper transformer layers:

$$\mathbf{g}^{(l)} \leftarrow \tau_l \cdot (\omega^{(l)} \cdot \mathbf{g}^{(l)})$$

3. **Feature-Sensitive Gradient Scaling (FSGS):** Token-level importance $\hat{\alpha}_i$ is computed from intermediate features, and each token’s gradient is scaled accordingly:

$$\mathbf{g}_i^{(l)} \leftarrow (\gamma_{\text{base}} + \lambda(1 - \hat{\alpha}_i)) \cdot \mathbf{g}_i^{(l)}$$

All module gradients are aggregated to form the total input gradient $\mathbf{g}^{(t)}$, and momentum is applied:

$$\mathbf{m}^{(t)} = \mu \cdot \mathbf{m}^{(t-1)} + \frac{\mathbf{g}^{(t)}}{\|\mathbf{g}^{(t)}\|_1}$$

The perturbation is updated and projected onto the ℓ_∞ -norm ball:

$$\delta^{(t)} = \text{Clip}_\epsilon \left(\delta^{(t-1)} + \eta \cdot \text{sign}(\mathbf{m}^{(t)}) \right)$$

Algorithm 1: TESSER: Transfer-Enhancing Adversarial Optimization from Vision Transformers via Spectral and Semantic Regularization

Input: Input \mathbf{x} , label y , model f , steps T , step size η , max perturbation ϵ , Gaussian blur \mathcal{G}_σ , momentum factor μ

Output: Adversarial example \mathbf{x}^{adv}

Initialize: $\delta^{(0)} = 0$, $\mathbf{m}^{(0)} = 0$;

for $t = 1$ **to** T **do**

$\mathbf{x}^{(t)} = \mathcal{G}_\sigma(\mathbf{x} + \delta^{(t-1)})$;

 Compute loss: $\mathcal{L}^{(t)} = \mathcal{L}(f(\mathbf{x}^{(t)}), y)$;

 Backpropagate with hooks at Attention, QKV, MLP ;

foreach *block* l **do**

 Extract features $\mathbf{z}^{(l)}$, gradients $\mathbf{g}^{(l)}$;

 Apply weakening: $\mathbf{g}^{(l)} \leftarrow \omega^{(l)} \cdot \mathbf{g}^{(l)}$;

 Apply layer modulation: $\mathbf{g}^{(l)} \leftarrow \tau_l \cdot \mathbf{g}^{(l)}$;

 Estimate token importance $\hat{\alpha}_i = \text{norm}(\mathbf{z}_i^{(l)})$;

 Apply FSGS: $\mathbf{g}_i^{(l)} \leftarrow (\gamma_{\text{base}} + \lambda(1 - \hat{\alpha}_i)) \cdot \mathbf{g}_i^{(l)}$;

end

 Aggregate total gradient $\mathbf{g}^{(t)}$ and update momentum:

$\mathbf{m}^{(t)} = \mu \cdot \mathbf{m}^{(t-1)} + \frac{\mathbf{g}^{(t)}}{\|\mathbf{g}^{(t)}\|_1}$;

 Update perturbation:

$\delta^{(t)} = \text{Clip}_\epsilon(\delta^{(t-1)} + \eta \cdot \text{sign}(\mathbf{m}^{(t)}))$;

end

return $\mathbf{x}^{\text{adv}} = \mathbf{x} + \delta^{(T)}$

Table 4: Model-specific hyperparameter settings used for TESSER. $\omega^{(\cdot)}$ denotes the weakening factor for each module, λ is the FSGS scaling parameter, σ controls the strength of spectral regularization, l_{cut} is the attention truncation depth, γ_{base} is the minimum gradient scaling factor, μ is the momentum decay used in PGD, and η is the step size for perturbation update.

Hyperparameter	ViT-B/16	PiT-B	CaiT-S/24	Visformer-S
$\omega^{(\text{attn})}$	0.45	0.25	0.3	0.4
$\omega^{(\text{qkv})}$	0.5	0.5	1.0	0.8
$\omega^{(\text{mlp})}$	0.7	0.7	0.6	0.5
λ_{attn}	0.4	0.45	0.5	0.45
λ_{qkv}	0.5	0.5	0.5	0.5
λ_{mlp}	0.55	0.55	0.65	0.6
σ (SSR)	0.5	0.7	0.7	0.7
l_{cut}	10	9	4	8
γ_{base}	0.5	0.5	0.5	0.5
μ	1.0	1.0	1.0	1.0
η	1.6/255	1.6/255	1.6/255	1.6/255

Description. Algorithm 1 summarizes our full optimization loop. The key innovation lies in the sequential application of module-wise weakening, layer-wise modulation, and semantic-aware scaling via FSGS. All components are implemented via backward hooks, ensuring compatibility with any transformer-based model.

Hyper-parameters. Table 4 summarizes the model-specific hyperparameters used in TESSER for each architecture. These include module-wise weakening factors ($\omega^{(\cdot)}$), FSGS scaling parameters (λ), spectral smoothness regularization strength (σ), attention truncation depth (l_{cut}), base gradient scaling (γ_{base}), as well as optimization parameters: momentum decay (μ) and step size (η). Values are carefully selected to balance gradient modulation and attack stability per architecture.

Table 5: Computational cost (in seconds) for generating a single adversarial example across different models and methods. FSGS refers to our feature-sensitive gradient scaling, SSR refers to spectral smoothness regularization, and ATT denotes state of the art.

Model	FSGS	FSGS + SSR	ATT [24]
ViT-B/16	0.5	0.52	0.93
PiT-B	0.54	0.6	1.05
CaiT-S/24	1.24	1.27	1.88
Visformer-S	0.35	0.38	1.14

B.2 Computational Cost

To evaluate the efficiency of our proposed method, we report the average time (in seconds) required to generate a single adversarial example using FSGS, FSGS+SSR, and the ATT across different models. As shown in Table 5, our methods incur minimal overhead compared to ATT, with only a slight increase when applying SSR. In particular, even in deeper architectures like CaiT-S/24, FSGS+SSR remains significantly more efficient than ATT.

We provide the detailed environment configuration used for all evaluations. All experiments were conducted on NVIDIA Tesla T4 GPUs hosted on Google Colab. We present the key software dependencies and their corresponding versions:

- Python: 3.11.12
- PyTorch: 2.6.0
- Torchvision: 0.21.0
- NumPy: 2.0.2
- Pillow: 11.2.1
- Timm: 1.0.15
- SciPy: 1.15.3

C Additional Experiments

C.1 Quantitative Analysis for SSR

To evaluate the effect of spectral regularization strength, we conduct an ablation study by varying the Gaussian blur standard deviation σ used in Spectral Smoothness Regularization (SSR). Table 6 reports the average attack success rates (ASR) on ViTs, CNNs, and defended CNNs for $\sigma \in \{0.5, 0.6, 0.7, 0.8\}$ across all surrogate models.

We observe a consistent trend: increasing σ improves transferability to CNNs and defended CNNs, while slightly reducing ASR on ViTs. This trade-off reflects the role of SSR in suppressing high-frequency architecture-specific noise: improving cross-architecture generalization but marginally weakening model-specific alignment. For instance, in ViT-B/16, increasing σ from 0.5 to 0.8 decreases ViT ASR from 83.21% to 81.21%, but improves CNN ASR from 58.77% to 61.82% and defended CNN ASR from 46.63% to 52.33%. A similar pattern is observed in PiT-B and CaiT-S/24.

Notably, the improvement on defended CNNs is particularly pronounced. For Visformer-S, the ASR on defended models improves from 46.96% at $\sigma = 0.5$ to 61.5% at $\sigma = 0.8$, a gain of over 14%. These results confirm that SSR strengthens black-box transferability and robustness by encouraging low-frequency perturbations that are less dependent on the surrogate model’s internal architecture.

In practice, setting σ between 0.6 and 0.8 offers a favorable trade-off, preserving sufficient ViT ASR while achieving substantial improvements on CNNs and defended models. This ablation supports the effectiveness of spectral regularization and its role in enhancing generalization under diverse adversarial settings.

Table 6: Average attack success rate (ASR) (%) against ViTs, CNNs, and defended CNNs across varying Gaussian blur strength σ . Increasing σ generally improves transferability to CNNs and defended models by enforcing low-frequency perturbations, while slightly reducing white-box ASR on ViTs.

Model	σ	ViTs	CNNs	Def-CNNs	Model	σ	ViTs	CNNs	Def-CNNs
ViT-B/16	0.5	83.21	58.77	46.63	CaiT-S/24	0.5	94.82	68.12	45.6
	0.6	83.12	61.85	49.86		0.6	94.57	71.9	51.76
	0.7	81.95	61.62	51.13		0.7	94.2	73.87	54.86
	0.8	81.21	61.82	52.33		0.8	93.82	73.55	57.06
PiT-B	0.5	90.3	80.85	49	Visformer-S	0.5	75.93	76.77	46.96
	0.6	91.63	83.4	54.9		0.6	78.47	80.45	53.9
	0.7	91.36	83.27	57.06		0.7	78.67	81.67	58.46
	0.8	90.02	83.45	58.6		0.8	83.33	81.22	61.5

Table 7: The average attack success rate (%) against ViTs, CNNs, and defended CNNs by various transfer-based attacks with input diversity enhancement strategy. The best results are highlighted in bold. ‘‘PO’’ denotes PatchOut [38].

Model	Attack	ViTs	CNNs	Def-CNNs	Model	Attack	ViTs	CNNs	Def-CNNs
ViT-B/16	MIM+PO	61.3	31.3	21.7	CaiT-S/24	MIM+PO	70.3	44.0	29.3
	VMI+PO	69.1	42.8	30.9		VMI+PO	76.8	57.8	38.4
	SGM+PO	64.8	29.2	18.9		SGM+PO	85.1	49.2	29.3
	PNA+PO	70.8	42.6	29.9		PNA+PO	81.6	56.6	39.3
	TGR+PO	76.0	46.7	33.3		TGR+PO	88.8	60.5	40.5
	ATT+PO	77.1	51.7	37.1		ATT+PO	91.1	71.9	54.3
	Ours+PO	85.18 \uparrow	64.17 \uparrow	52.16 \uparrow		Ours+PO	91.15 \uparrow	72.9 \uparrow	56.46 \uparrow
PiT-B	MIM+PO	47.3	32.5	17.5	Visformer-S	MIM+PO	54.9	45.7	23.4
	VMI+PO	59.5	46.2	35.8		VMI+PO	64.8	56.6	32.6
	SGM+PO	70.0	45.6	21.3		SGM+PO	51.6	44.3	15.0
	PNA+PO	73.1	57.8	32.7		PNA+PO	68.8	61.8	32.3
	TGR+PO	82.3	68.9	41.3		TGR+PO	70.4	64.3	33.5
	ATT+PO	84.2	75.2	48.4		ATT+PO	70.5	79.3	44.5
	Ours+PO	94.83 \uparrow	87.7 \uparrow	61.43 \uparrow		Ours+PO	84.42 \uparrow	79.4 \uparrow	58.06 \uparrow

C.2 Comparison of Attack Efficiency when using Input Diversity Technique

To further assess the effectiveness and generality of our proposed TESSER framework, we evaluate its performance when combined with an input diversity enhancement strategy, specifically PatchOut (PO) [38]. This technique introduces random masking during inference to improve the robustness and transferability of adversarial perturbations.

Table 7 presents the average Attack Success Rate (ASR) of different attack methods augmented with PO, tested across ViTs, CNNs, and defended CNNs. The experiments span four representative surrogate models: ViT-B/16, CaiT-S/24, PiT-B, and Visformer-S.

Across all surrogate models and evaluation categories, TESSER+PO consistently achieves the highest ASR. For example, using PiT-B as the surrogate, TESSER+PO achieves an ASR of **94.83%** on ViTs, **87.7%** on CNNs, and **61.43%** on defended CNNs, representing improvements of more than **+10%** over the strongest baseline ATT+PO. Similar trends are observed with the other surrogate models, including CaiT-S/24 and ViT-B/16, where TESSER+PO continues to outperform baselines by wide margins.

These results demonstrate two key insights: (1) TESSER is orthogonal to input diversity methods, as its performance improves further when used with PO, and (2) our gradient modulation and spectral regularization strategies remain effective under randomized input transformations, indicating strong generalization.

In particular, on defended CNNs, traditionally difficult targets due to adversarial training, TESSER + PO outperforms all baselines by significant margins (e.g., +7% over ATT + PO with ViT-B/16). This highlights that FSGS and SSR lead to perturbations that survive stochastic augmentations while preserving transferability and robustness.

Table 8: Comparison of attack efficiency and effectiveness between TESSER and ATT. We report the average iteration where the model prediction stabilizes on the adversarial label (lower is better) and the final model confidence (%) in the adversarial class (higher is better).

Method	Stabilization Iteration (↓)	Final Confidence (%) (↑)
ATT	6.8	87.93
TESSER (Ours)	5.1	91.37

C.3 Adversarial Attack Efficiency and Confidence Dynamics

To better assess the quality of adversarial examples beyond final attack success rate (ASR), we evaluate the efficiency and effectiveness of the generated perturbations in terms of iteration-wise model response. Specifically, we compare TESSER and ATT based on:

- **Attack efficiency:** How quickly the model’s prediction flips and stabilizes to an adversarial label across iterations.
- **Attack effectiveness:** The final confidence of the model in the adversarial label after optimization completes.

Table 8 summarizes the average iteration at which the target model stabilizes on the adversarial label (i.e., no further label flipping) and the average confidence on the adversarial class after 10 attack steps.

TESSER reaches a stable adversarial label approximately 1.7 iterations earlier than ATT, confirming its improved gradient alignment and optimization direction. Additionally, the final adversarial confidence achieved by TESSER is consistently higher, indicating stronger and more decisive misclassification. This validates that our semantic gradient modulation not only accelerates convergence but also increases attack effectiveness by pushing perturbations toward model-relevant, transferable features.

D Additional Ablation Studies

To further analyze the effectiveness and interpretability of our proposed method, we present qualitative comparisons between TESSER (FSGS+SSR) and the state-of-the-art ATT [24] across a diverse set of samples from ImageNet. Figure 3 shows clean and adversarial images, Grad-CAM heatmaps, and FFT visualizations for perturbations.

Semantic Alignment. In nearly all examples, the adversarial images generated by TESSER show stronger alignment with semantically meaningful regions (e.g., bird bodies, faces, objects of interest) compared to ATT. This is reflected in the Grad-CAM visualizations guided by the adversarial label. Despite being misclassified, the Grad-CAM of TESSER adversarial examples remains spatially focused on relevant visual features, validating the effectiveness of FSGS in preserving semantically informative gradients during attack optimization.

Spectral Coherence. The FFT visualizations reveal that TESSER perturbations exhibit smoother and more coherent frequency profiles, with lower high-frequency energy content than those generated by ATT. This is consistently supported by the computed High-Frequency Energy Ratio (HFER), which is reduced by 6–16% across examples when using FSGS+SSR. Lower HFER confirms that SSR suppresses architecture-specific, high-frequency noise that often undermines transferability.

These additional ablations reinforce our core claim: FSGS guides perturbations toward transferable, semantically meaningful features, while SSR regularizes their spectral profile to avoid overfitting to model-specific noise. Together, these properties lead to adversarial examples that are more interpretable and more effective in black-box transfer scenarios.

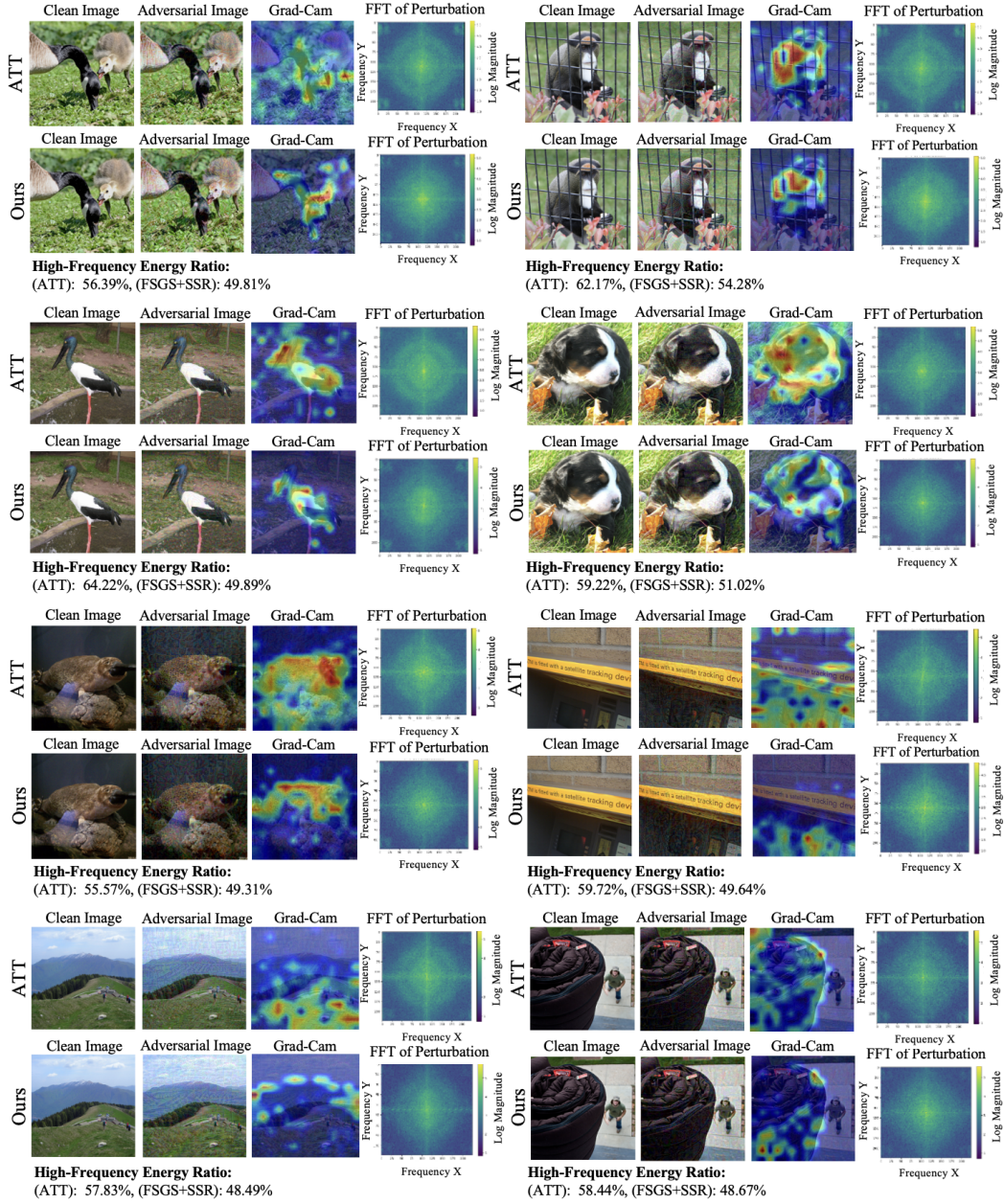


Figure 3: Qualitative comparison between ATT and our TESSER method (FSGS+SSR). Each block shows clean image, adversarial image, Grad-CAM heatmap, and FFT of the perturbation. TESSER yields semantically aligned and spectrally smooth perturbations, with consistently lower high-frequency energy ratios.